HHS Public Access

Author manuscript

Clin Cancer Res. Author manuscript; available in PMC 2022 July 01.

Published in final edited form as:

Clin Cancer Res. 2022 January 01; 28(1): 201–214. doi:10.1158/1078-0432.CCR-21-1248.

Targeting Fc receptor-mediated effects and the "don't eat me" signal with an oncolytic virus expressing an anti-CD47 antibody to treat metastatic ovarian cancer

Lei Tian[#,1], **Bo Xu**[#,1], **Kun-Yu Teng**[1], **Mihae Song**[2], **Zheng Zhu**[1], **Yuqing Chen**[1], **Jing Wang**[1], **Jianying Zhang**[3], **Mingye Feng**[4], **Balveen Kaur**[5], **Lorna Rodriguez**[2], **Michael A Caligiuri**[1,4,6,7,*], **Jianhua Yu**[1,4,6,7,*]

[1]Department of Hematology and Hematopoietic Cell Transplantation, City of Hope National Medical Center, Los Angeles, California, USA.

[2]Department of Surgery, Division of Gynecologic Oncology, City of Hope National Medical Center, Los Angeles, California, USA.

[3]Department of Computational and Quantitative Medicine, City of Hope National Medical Center, Los Angeles, California, USA.

[4]Department of Immuno-Oncology, Beckman Research Institute, City of Hope Comprehensive Cancer Centre, Los Angeles, California, USA.

[5]Department of Neurosurgery, McGovern Medical School, University of Texas, University of Texas Health Science Center at Houston, Houston, Texas, USA.

[6]Hematologic Malignancies Research Institute, City of Hope National Medical Center, Los Angeles, California, USA.

[7]City of Hope Comprehensive Cancer Center, Los Angeles, California, USA.

Abstract

Purpose: Monoclonal antibodies (mAbs) blocking immune checkpoints have emerged as important cancer therapeutics, as exemplified by systemic administration of the IgG1 anti-CD47 mAb that blocks the "don't eat me" pathway. However, this strategy is associated with severe toxicity.

Experimental Design: To improve therapeutic efficacy while reducing toxicities for ovarian cancer, we engineered an oncolytic herpesvirus (oHSV) to express a full-length, soluble anti-CD47 mAb with a human IgG1 scaffold (OV-αCD47-G1) or IgG4 scaffold (OV-αCD47-G1).

[*]Corresponding authors. Michael A Caligiuri, MD, mcaligiuri@coh.org; Jianhua Yu, PhD, jiayu@coh.org.
[#]These authors equally contributed to this work.

Authors' Contributions

J. Yu, M.A. Caligiuri, L. Tian, and B. Xu conceived and designed the project. J. Yu, M.A. Caligiuri, L. Tian, B. Xu, K. Teng, Z, Zheng, Y. Chen, and J. Wang designed and/or supervised experiments. L. Tian and J. Zhang performed data analyses. L. Tian, M, Song, M, Feng, B. Kaur, L, Rodriguez, J. Yu, and M.A. Caligiuri wrote, reviewed, and/or revised the paper. All authors discussed the results and commented on the manuscript.

Declaration of Interests

Drs. Caligiuri and Yu are cofounders of CytoImmune Therapeutics, Inc. Other authors have no conflict of interest to declare.

Results: Both IgG1 and IgG4 anti-CD47 mAbs secreted by oHSV-infected tumor cells blocked the CD47-SIRPα signal pathway, enhancing macrophage phagocytosis against ovarian tumor cells. OV-αCD47-G1, but not OV-αCD47-G4, activated human NK cell cytotoxicity and macrophage phagocytosis by binding to the Fc receptors of these cells. *In vivo*, these multifaceted functions of OV-αCD47-G1 improved mouse survival in xenograft and immunocompetent mouse models of ovarian cancer when compared to OV-αCD47-G4 and a parental oHSV. The murine counterpart of OV-αCD47-G1, OV-αmCD47-G2b, also enhanced mouse NK cell cytotoxicity and macrophage phagocytosis and prolonged survival of mice bearing ovarian tumors compared to OV-αmCD47-G3. OV-αmCD47-G2b was also superior to αmCD47-G2b and showed a significantly better effect when combined with an antibody against PD-L1 that was upregulated by oHSV infection.

Conclusion: Our data demonstrate that an oHSV encoding a full-length human IgG1 anti-CD47 mAb, when used as a single agent or combined with another agent, is a promising approach for improving ovarian cancer treatment via enhancing innate immunity, as well as performing its known oncolytic function and modulation of immune cells.

Introduction

Ovarian cancer is the most lethal gynecologic malignancy (1–3). Although the majority of women with ovarian cancer initially respond to surgery and platinum-based chemotherapy, over 80% develop platinum-resistance, relapse, and die. Women with platinum-resistant tumors have poor prognosis as current treatments are usually ineffective. Increasing evidence from preclinical and clinical data indicates that immunotherapeutic approaches that harness and enhance anti-tumor effector cells, such as immune checkpoint blockade and specific monoclonal antibody (mAb) therapy, have led to clinical benefits for ovarian cancer (4).

CD47 was first identified as a tumor antigen on human ovarian cancer in the 1980s, and its overexpression is associated with a poor prognosis in ovarian cancer (5–7). CD47 provides a “don’t eat me” signal when it binds to its receptor, signal regulatory protein alpha (SIRPα), on macrophages, thereby suppressing phagocytosis (8–10). Anti-CD47 antibodies, including the human IgG1 scaffold and IgG4 scaffold, are being actively tested in clinical trials (11,12).

The traditional methods of delivering therapeutic mAb or mAb-drug conjugates often result in a limited distribution to tumor tissue and frequently create systemic toxicity due to off-tumor, on-target effects, or Fc receptor-mediated activation of innate immune effector cells (13,14). However, oncolytic virus (OV) is an ideal carrier that is able to specifically deliver a payload into the tumor environment after administration (15). More importantly, the infection of OV can dramatically activate immune responses at the local tumor microenvironment, in turn, improving the efficacy of the antibody or other payloads delivered with the OV (15–18).

In this study, we generated novel oncolytic herpes viruses (oHSV) termed OV-aCD47-G1 encoding a full-length anti-CD47 antibody on a human IgG1 scaffold (αCD47-G1) and OV-aCD47-G4 encoding a full-length anti-CD47 antibody on a human IgG4 scaffold (αCD47-G4). Both OV-αCD47-G1 and OV-aCD47-G4 blocked the “don’t eat me” signal

of macrophages, but only OV-αCD47-G1 induced antibody-dependent cellular phagocytosis (ADCP) of macrophages and antibody-dependent cellular cytotoxicity (ADCC) of NK cells targeting ovarian cancer cells. In ovarian cancer mouse models, the administration of OV-αCD47-G1 or the mouse counterpart, OV-αmCD47-G2b significantly inhibited local tumor growth as well as had an abscopal effect in an ovarian cancer metastasis mouse model.

Materials and Methods

Ethics statement.

All experiments and animal handling were conducted under federal, state, and local guidelines and with approval from the City of Hope Animal Care and Use Committee. Peripheral blood cones were collected from healthy donors with a written informed after written informed consent under a protocol approved by the City of Hope Institutional Review Board.

Cells

The human ovarian cancer cell line A2780, the Chinese hamster ovary cell line CHO, the monkey kidney epithelium-derived Vero cell line, and the mouse ovarian cancer cell line ID8 were cultured with DMEM supplemented with 10% FBS, penicillin (100 U/ml), and streptomycin (100 μg/ml). CHO cells were used for producing αCD47-G1 and αCD47-G4 antibodies. Vero cells were used for viral propagation and plaque-assay-based viral titration. The A2780 cell line was a recent gift from Dr. Edward Wang's lab at City of Hope. The CHO cell line was recently purchased from American Type Culture Collectio (ATCC). All cell lines used in this study were not authenticated upon receipt but are routinely tested for the absence of mycoplasma by using the MycoAlert Plus Mycoplasma Detection Kit from Lonza (Walkersville, MD).

Generation of OV-αCD47-G1, OV-αCD47-G4, OV-αmCD47-G2b and OV-αmCD47-G3

OV-αCD47-G1, OV-αCD47-G4, OV-αmCD47-G2b, and OV-αmCD47-G3 were generated by using a published protocol with slight modifications (15,19). For expressing full-length αCD47-G1 and αCD47-G4 simultaneously in the viral vector, a DNA sequence encoding a T2A self-cleaving peptide was used to link the light chain and heavy chain coding genes. For expressing αmCD47-G2b and αmCD47-G3 in the viral vector, a mouse anti-CD47 antibody single-chain variable fragment was fused with different mouse IgGs. The engineered viral vectors were recombined with fHsvQuik-1 for engineering the corresponding oHSV. Virus titration was performed using plaque assays using Vero cells, as we previously reported (15,18). The viral particle purification and concentration were conducted also following the published protocol (15,18).

Measurement of antibody concentration

A2780 cells were saturated infected with OV-Q1, OV-αCD47-G1, or OV-αCD47-G4. Two hours post infection, the infection media were changed with DMEM supplemented with 10% FBS. The supernatants from each group were collected at 6, 12, 24, 48, and 72 hours post infection. The antibody concentrations of the indicated timepoints were measured by ELISA as previously reported with slight modification (20). The standard curve was

constructed with αCD47-G1 and αCD47-G4 antibodies purified from CHO cells with known concentrations with the recombinant human CD47 protein (Abcam, ab174029) used as a coating reagent. The anti-human Fc antibody (sigma, MAB1307) was the detecting antibody.

To compare the concentration of αmCD47-G2b at tumor sites in the abdomen and the systemic bloodstream, six- to eight-week-old female C57BL/6 mice were i.p injected with 2×10^6 wild type ID8 cells at day 0. At day 4, mice were randomly divided into groups that were i.p injected with either 1×10^6 PFU OV-Q1 or the same amount of OV-αmCD47-G2b in 100 μl saline. Saline alone was used as a placebo control. Mice were euthanized at days 5, 6, 7, and 10. The peripheral blood and tumors in the abdomen were collected. Sera were prepared from the peripheral blood and the tumors were homogenized for ELISA assay to detect the concentrations of αmCD47-G2b. The ELISA standard curve was constructed with αmCD47-G2b antibodies purified from CHO cells with known concentrations determined by NanoDrop One (Thermo Scientific). The recombinant mouse CD47 protein (Abcam, ab231160) served as a coating reagent and the anti-mouse Fc antibody (Invitrogen, 31439) was the detecting antibody.

Oncolysis assay

The *in vitro* oncolysis assay was measured by real-time cell analysis (RTCA) using xCELLigence RTCA MP instrument. Briefly, A2780 cells were seeded onto 96-well plates at densities of 5,000 cells/well and allowed to attach for 24 hours. Cells were then treated with graded concentrations of OV-Q1, OV-αCD47-G1, or OV-αCD47-G4. The oncolysis assay was monitored and analyzed with RTCA software (ACEA Biosciences, Agilent).

Macrophage generation

For isolating and culturing human primary macrophages, human monocytes were isolated from peripheral blood of healthy donors and enriched by using the RosetteSep™ Human Monocyte Enrichment Cocktail kit (Stemcell, Cat#15068) RPMI-1640 medium containing 20 ng/ml human M-CSF (PeproTech, Cat#300–25-50UG) and 2% human serum was used to differentiate monocytes into macrophages.

Murine bone marrow-derived macrophages (BMDMs) were isolated from BALB/c mice and induced differentiation by RPMI-1640 medium containing 10 ng/ml murine M-CSF (PeproTech, Cat# 315–02-50UG) and 10 % FBS.

Flow cytometry-based phagocytosis assay

For the phagocytosis assay of human primary macrophage, A2780 cells prelabeled with CFSE (Thermo Fisher, C34554) were cocultured with human macrophages at a ratio of 2:1 for 4 hours in the presence of vehicle control, αCD47-G1 or αCD47-G4 at the dose of 5 μg/ml or supernatants of OV-infected cells at 37 °C in ultra-low-attachment 96-well U-bottom plates (Corning) in serum-free 1640 (Life Technologies). Then the cells were harvested and stained with anti-human CD45 (BD, 552850) to identify macrophages. All flow cytometry data were collected using a Fortessa X20 flow cytometer (BD Biosciences).

Phagocytosis was calculated as the number of $CD45^+CFSE^+$ macrophages, quantified as a percentage of the total $CD45^+$ macrophages.

For the phagocytosis of mouse macrophages, ID8 or A2780 cells prelabeled with CFSE were cocultured with murine macrophages at a ratio of 2:1 for 6 hours with 5 μg/ml antibodies or supernatants of OV-infected cells at 37°C in ultra-low-attachment 96-well U-bottom plates (Corning) in the serum-free 1640 media (Life Technologies). The cells were harvested. An anti-mouse F4/80 antibody (BD, cat#565787) was used to identify macrophages. Phagocytosis was measured as the number of $F4/80^+CFSE^+$ macrophages and quantified as a percentage of the total $F4/80^+$ macrophages.

Quantitative PCR

For evaluating the effect of αCD47-G1 and αCD47-G4 on activating transcription of typical human macrophage cytokine genes, human macrophages and A2780 cells were cocultured at a ratio of 1:1 for 6 hours with or without 5 μg/ml αCD47-G1 or αCD47-G4. Then human macrophages were FACS-sorted by staining with an anti-CD45 antibody using a BD Aria Fusion flow cytometer. The total RNA was extracted for measuring the relative transcription of human *IL1B, IL6, IL10, IL12A, Arg1, TNF, CCL2, CD206,* and *NOS2* genes with a pair of corresponding primers for each gene. 18s rRNA was used as an internal control (Supplemental Table 1).

NK cell cytotoxicity and activation assay

A2780 cells prelabeled with ^{51}Cr were used as target cells. Effector cells were primary human NK cells isolated from peripheral blood cones using an NK cell isolation kit (MACSxpress Miltenyi Biotec, San Diego, CA) and an erythrocyte depletion kit for the removal of red blood cells (Miltenyi Biotec). The target cells were incubated with 1 μg/ml αCD47-G1 or αCD47-G4 antibodies or vehicle for 30 min. Then the target cells were cocultured with isolated human primary NK cells at different effector: target ratios at 37 °C for 4 h. Release of ^{51}Cr was measured with a MicroBeta^2 microplate radiometric counters (Perkin Elmer, Waltham, MA). The cytotoxicity was calculated as previously report (15,21). At least three technical replicates with NK cells from different donors were performed. The expression of CD69 and granzyme B of NK cells were measured 12 hours after coculturing withA2780 cells with or without 1 μg/ml αCD47-G1 or αCD47-G4 antibodies or 100 μL supernatants derived from OV-Q1-, OV-αCD47-G1- and OV-αCD47-G4-infected A2780 ovarian cancer cells at 48-hour post infection at a ratio of 1:1 by flow cytometry after being stained with the anti-CD56 antibody (BD, cat#557919), anti-granzyme B antibody, anti-CD69 (BD, cat#562883) antibody. Other NK cell activation markers were measured 12 hours after coculturing A2780 cells with or without 1 μg/ml αCD47-G1 or αCD47-G4 antibodies or 100 μL supernatants derived from OV-Q1-, OV-αCD47-G1- and OV-αCD47-G4-infected A2780 ovarian cancer cells at 12-hour post infection at a ratio of 1:1 by flow cytometry after being stained with the anti-CD56 antibody (BD, cat#557919), anti-4–1BB antibody (Biolegend, cat#309804), anti-CD107a antibody (BD, cat#555800), anti-CD27 antibody (Biolegend, cat#356404), anti-CD11b antibody (Biolegend, cat#301306), and anti-Ki67 antibody (BD, cat# 564071).

Animal Studies

Six- to eight-week-old female athymic nude mice were purchased from Jackson Laboratories (Bar Harbor, Maine). For survival studies in an immunodeficient model, mice were anesthetized and s.c. injected with 5×10^6 A2780 cells into the right flank. One day after A2780 cells injection, animals were subsequently randomly divided into groups that were injected intratumorally either with 2×10^5 PFU oHSV (OV-Q1, OV-αCD47-G1 or OV-αCD47-G4) in 10 μl of saline or with saline as control. Mice were subsequently monitored for ovarian cancer progression. Mice were euthanized when the diameter of tumors was over 15 mm.

For establishing the immunocompetent mouse ovarian tumor model, six- to eight-week-old female C57BL/6 mice were purchased from Jackson Laboratories (Bar Harbor, Maine). The mice were anesthetized and i.p injected with 2×10^6 wild-type ID8 cells or ID8-hCD47 cells, which express the human CD47 gene. After the cells grew for 3 days *in vivo*, mice were randomly divided into groups that were i.p injected either with 1×10^6 PFU oHSV (OV-Q1, OV-αCD47-G1, OV-αCD47-G4, OV-αmCD47-G2b, or OV-αmCD47-G2b) in 100 μl of saline. Saline alone was used as a placebo control. Mice were subsequently monitored and weighed frequently to monitor ovarian cancer disease progression. Luciferase-based *in vivo* images were taken after tumor implantation to evaluate the tumor development. Mice were euthanized when they became moribund.

Flow cytometry

Mononuclear cells in the tumor site, liver, and kidney were extracted with Percoll and stained with anti-NKp46 (Biolegend, cat#137618), anti-CD3 (BD, cat#553066), anti-CD45 (BD, cat#559864), anti-CD11b (BD, cat#552850), anti-F4/80 (Thermo, cat# 12–4801-82), anti-CD4 (BD, cat# 557308) and anti-CD8 (BD, cat# 553030), anti-CD86 (BD, cat#740900), anti-CD206 (Biolegend, cat#141734), anti-CD69 (BD, cat#564683), anti-IFNγ (BD, cat#563773), anti-granzyme B (Thermo Fisher, cat#48–8898-82) antibodies for flow cytometric analysis of immune cell infiltration and activation. H-2K(b) herpes simplex virus type 1 glycoprotein B tetramer was provided by the NIH Tetramer Core Facility. The flow cytometric assessments of murine immune cells were performed with at least 3 independent animals. All flow cytometry data were collected using the Fortessa X-20 flow cytometer except cell sorting experiments that were performed using FACS Aria II cell sorter (BD Biosciences).

Statistical analysis

For continuous endpoints that are normally distributed, data are presented as mean ± standard deviations (SD). Student's t test was used to compare two independent conditions, and one-way ANOVA was used to compare three or more conditions. For data with repeated measures from the same subject/donor, a linear mixed model was used to account for the underlying variance and covariance structure. P values were adjusted for multiple comparisons by Holm's procedure or the Bonferroni method, and a P value of 0.05 or less was defined as statistically significant. For survival data, survival functions were estimated by the Kaplan–Meier method and compared by log-rank test. All tests were two-sided. Statistical software GraphPad, R.3.6.3. and SAS 9.4 were used for the statistical analysis.

Results

Construction and characteristics of OV-αCD47-G1 and -G4

We first demonstrated a high surface expression of CD47 on the human ovarian cancer cell line A2780 (Fig. 1A). We generated IgG1 and IgG4 versions of the humanized anti (α)-human CD47 antibody. We reconstructed αCD47-G4 by following the previously reported method (22). The human IgG4 constant region of αCD47-G4 was replaced by the human IgG1 for constructing αCD47-G1. CHO cells were transduced with lentiviral vectors carrying the corresponding constructs to produce αCD47-G1 or αCD47-G4. To assess the specificity of these mAbs, A2780 cells were first incubated with the increasing concentrations of αCD47-G1 or αCD47-G4 antibodies purified from the lentiviral-infected CHO cells, followed by staining with a BV786-conjugated anti-CD47 antibody (clone: B6H12). Results showed a similar dose-dependent decrease of BV786 signal when the cells were preincubated with increasing concentrations of either αCD47-G1 or αCD47-G4, indicating that both αCD47-G1 and αCD47-G4 have similar recognition of CD47 that blocks CD47 binding to SIRPα (Fig. 1B). OV-αCD47-G1- and OV-αCD47-G4 were constructed by inserting the coding genes of αCD47-G1 and αCD47-G4 into the oHSV backbone (OV-Q1), respectively, driven by the immediately early gene promoter IE4/5 of the virus to get a high-level expression after infection. The construction of OV-αCD47 is shown in Supplementary Fig.1. When the human ovarian cancer cell line A2780 was infected by OV-αCD47-G1 or OV-αCD47-G4 at a multiplicity of infection (MOI) of 2, anti-CD47 antibodies were detected in supernatants of infected cells as early as 6 hours after infection, reaching a concentration of > 5 μg/ml at 24 hours (Fig. 1C). We next assessed whether the inserted gene encoding the anti-CD47 antibody into the oHSV adversely affected the tumor lysis capability of OV-αCD47-G1 or OV-αCD47-G4 when compared to the parental oHSV, OV-Q1. When A2780 cells were infected with varying titers of OV-αCD47-G1, OV-αCD47-G4, or OV-Q1, there was no obvious difference in cell death or oncolysis among the three groups tested (Fig. 1D). Therefore, the insertion of αCD47-G1 and αCD47-G4 coding genes does not affect the oncolytic ability of OV-αCD47-G1 and OV-αCD47-G4 *in vitro*.

αCD47-G1 activates stronger anti-tumor effects in macrophages than αCD47-G4

We next determined the effect of αCD47-G1 and αCD47-G4 purified from the lentiviral-infected CHO cells on human macrophage phagocytosis. Both αCD47-G1 and αCD47-G4 effectively induced human macrophage phagocytosis against A2780 ovarian cancer cells compared to control, but αCD47-G1 performed significantly better than αCD47-G4 (Fig. 2A–B). Next, we repeated this experiment with supernatants from OV-αCD47-G1-, OV-αCD47-G4- or OV-Q1-infected A2780 cells. The results showed that supernatants from OV-αCD47-G1-infected cells significantly enhanced macrophage phagocytosis against A2780 ovarian cancer cells compared to supernatants from OV-Q1- and OV-αCD47-G4-infected cells (Fig. 2C–D). Similar results were obtained with bone marrow-derived macrophages (BMDMs) isolated from BALB/c mice using the antibodies purified from lentiviral-infected CHO cells as well as supernatants from OV-infected A2780 cells (Fig. 2E–H). For both murine and human macrophages, the increased phagocytotic effect of αCD47-G1 compared

to vehicle control should result from both the blockade of “don’t eat me” signaling and ADCP, while the increased effect compared to αCD47-G4 should be mainly from ADCP.

The effects of CHO-derived αCD47-G1 and αCD47-G4 on regulating the cytokine expression of human macrophages were assessed. Human macrophages were incubated with A2780 cells in the presence of αCD47-G1, αCD47-G4, or vehicle for 6 hours, followed by total RNA extraction and quantitative assessment of cytokine transcripts. Compared to αCD47-G4, αCD47-G1 dramatically increased the transcription of macrophage cytokine genes such as *IL6*, *IL10*, *NOS2, TNF,* and *IL12A,* which are also macrophage M1 markers; however, the transcription of *IL1B* and *CCL2* was similar in both treatment groups. Furthermore, αCD47-G1 and αCD47-G4 had no regulatory effect on M2 macrophage markers, including *Arg1* and *CD206* (Fig. 2I and Fig. S2).

OV-αCD47-G1 activates the anti-tumor effect of human NK cells.

NK cells have an anti-tumor function because of their natural cytotoxicity and ADCC in the presence of some antibodies. To determine the effect of αCD47-G1 and αCD47-G4 on NK cell anti-tumor activity, we performed NK cell cytotoxicity assays using freshly isolated human NK cells as effector cells and A2780 ovarian cancer cells as target cells. The results showed that αCD47-G1 but not αCD47-G4 induced strong NK cell ADCC against ovarian cancer cells (Fig. 3A). Next, supernatants from OV-Q1-, OV-αCD47-G1- and OV-αCD47-G4-infected A2780 ovarian cancer cells were used to repeat this experiment, with comparable results, i.e., only supernatants from OV-αCD47-G1-infected A2780 cells induced strong NK cell cytotoxicity compared to the OV-Q1 or OV-αCD47-G4 supernatants (Fig. 3B). Furthermore, in the presence of tumor cells, αCD47-G1 but not αCD47-G4 significantly increased the surface expression of the activation marker CD69 on NK cells (Fig. 3C–D), and stronger effects were seen when using supernatants from OV-Q1-, OV-αCD47-G1- and OV-αCD47-G4-infected A2780 ovarian cancer cells (Fig. 3E–F), likely because we used the 1 μg/ml antibody concentration was used in Figure 3C–D while the concentration in Figure 3E–F was >5 μg/ml (Fig. 1C). Both αCD47-G1 and αCD47-G4 significantly upregulated the production of granzyme B in NK cells compared to the control, but αCD47-G1 treatment showed a significantly stronger activated effect on the production of granzyme B in NK cells compared to αCD47-G4 treatment (Fig. 3G–H). We also analyzed Ki67, NKG2D, 4–1BB, CD27, CD11b, CD107a, and IFNγ expression of NK cells. In the presence of tumor cells, αCD47-G1 but not αCD47-G4 significantly increased the surface expression of CD27, 4–1BB, and CD107a on NK cells but had no effect on regulating Ki67, NKG2D, CD11b, and IFNγ expression (Fig. S3A–C). Similar results were seen when using supernatants from OV-Q1-, OV-αCD47-G1- and OV-αCD47-G4-infected A2780 ovarian cancer cells (Fig. S3D–E).

OV-αCD47-G1 improves the therapeutic efficacy against ovarian cancer *in vivo* locally and abscopally and promotes macrophage M1 polarization and NK cell activation

To evaluate the efficacy of OV-αCD47-G1 and OV-αCD47-G4 in an ovarian cancer mouse model, we utilized a previously described xenograft model of ovarian cancer by s.c. injecting 5×10^6 A2780 cells into nude mice (23). One day after tumor implantation, animals received an intratumoral injection with OV-αCD47-G1, OV-αCD47-G4, or OV-Q1 at the

dose of 2×10^5 plaque-forming unit (PFU) per mouse, or saline as a placebo control. Tumor progression was monitored by measuring the tumor size with a caliper. OV-αCD47-G1 was significantly more effective than OV-αCD47-G4 and OV-Q1 at inhibiting the progression of tumors and prolonging the survival of mice *in vivo* (Fig. 4A and Fig. S4A). OV-Q1 moderately slowed tumor progression compared to vehicle control (Fig. 4A–C).

Metastatic ovarian cancer is an advanced stage malignancy that has spread from the cells in the ovaries to distant areas of the body, including the abdomen, liver, and kidney. To evaluate the role of OV in an ovarian cancer metastasis mouse model, we first detected the virus distribution after OV-Q1 intraperitoneal (i.p) administration. The virus titer in the liver and kidney was measured by q-PCR. Compared to the saline group, the OV group had high titers of the virus in the liver and kidney (Fig. S5A), suggesting that OV might have an abscopal effect in controlling metastatic tumors. We next sought to evaluate the efficacy of OV-αCD47-G1 in an immunocompetent ovarian cancer metastasis mouse model. Mouse firefly luciferase (FFL) gene-expressing ID8 ovarian cancer cells were modified to express human CD47 (referred to as ID8-hCD47-FFL cells) so that OV-αCD47-G1 can bind to hCD47 on tumor cells. ID8-hCD47-FFL cells also expressed the GFP marker for a tracing purpose. For establishing a mouse model that can be used to test OV-αCD47-G1 and -G4, ID8-hCD47-FFL cells were injected i.p. into immunocompetent wild-type C57BL/6 mice on day 0. On day 4, mice were randomly grouped and treated i.p with 1×10^6 PFU OV-Q1, OV-αCD47-G1, OV-αCD47-G4, or saline. Tumor progression was monitored by luciferase-based imaging on days 10 and 20 post tumor implantation. Mice treated with OV-αCD47-G1 significantly prolonged their median survival when compared to mice treated with OV-αCD47-G4 or OV-Q1 (Fig. 4C and Fig. S5B). However, there was no significant difference between OV-αCD47-G4 and OV-Q1 treatments, mainly because of the murine macrophages still receiving the murine-CD47-mediated “don’t eat me” signal from the ID8-hCD47-FFL cells, which cannot be blocked by human αCD47-G1 or αCD47-G4. Bioluminescent imaging data and sizes of representative tumors in the abdomen confirmed this result (Fig. S5B and S5C). Tumor cells were also detected in the liver and kidney in this ID8-hCD47 immunocompetent metastatic ovarian cancer model. The injections of each OV reduced the tumor burden in the liver and kidney, with a significantly more profound effect for OV-αCD47-G1 than OV-αCD47-G4 and OV-Q1 (Fig. 4D, S5D and S5E). For evaluating the immune responses, cells isolated from the tumor, liver, and kidney were collected then subjected to FACS analysis. Compared to the saline group, more NK cells and T cells infiltrated into tumors in the abdomen of OV-treated mice, but there were no differences among the three OVs (Fig. S6A and S7A). It has been reported that anti-CD47 antibody treatment stimulates phagocytosis of glioblastoma by promoting macrophages polarizing towards M1 type *in vivo* (24). Therefore, we detected the M1 (as a marker of CD86) and M2 (as a marker of CD206) macrophages in the tumor. Flow cytometry data showed that OV-αCD47-G1 treatment significantly decreased the number of M2 type macrophages but increased M1 type macrophages, when compared to the other treatments (Fig. 4E and S8A). OV-αCD47-G4 decreased the M2 type macrophages but showed a negligible effect on regulating M1 type macrophages when compared to OV-Q1 treatment (Fig. 4E and S8A). Our data indicated that OV-αCD47-G1 treatment promoted macrophages polarizing towards M1 type *in vivo*. The activation status of NK cells *in vivo*, indicated by the percentages

of CD69$^+$ NK cells, was also analyzed. Compared to saline, OV-Q1, and OV-αCD47-G4, OV-αCD47-G1 treatment increased the percentages of CD69$^+$ NK cells, indicating that OV-αCD47-G1 administration activated NK cells *in vivo* (Fig. 4F and S8A). Significantly more macrophages, NK cells, and T cells infiltrated into the liver in the OVs-treated mice vs. saline-treated mice (Fig. S6B and S7B). Although there was no difference in percentages of infiltrated immune cells in the liver among three viruses, M1 type macrophages and activated NK cells were increased in the OV-αCD47-G1 group, compared to the OV-Q1- or OV-αCD47-G4-treated group (Fig. 4G, 4H and S8B). Similar results for immune cell infiltration and cell activation were found in the kidney (Fig. S6C, S7C–E and S8C). Collectively, our data suggest that OV-αCD47-G1 is superior to OV-αCD47-G4 or OV-Q1 for improving oncolytic virotherapy in an immunocompetent ovarian cancer metastasis mouse model as it more effectively polarizes macrophages toward the M1 type and activates NK cells.

OV-αmCD47-G2b enhances the therapeutic efficacy in a fully immunocompetent ovarian cancer metastasis mouse model

To confirm our data, we generated the murine counterpart of OV-αCD47-G1 and OV-αCD47-G4 using the sequences of a murine anti-CD47 antibody (25). According to the binding affinity between mouse IgG and its Fc receptors, αmCD47-IgG2b version and αmCD47-IgG3 version were engineered, corresponding to human αCD47-G1 and OV-αCD47-G4, respectively (26). For assessing the specificity of αmCD47 antibody, ID8 cells were first incubated with increasing concentrations of αmCD47-G2b antibodies purified from the lentiviral-infected CHO cells, followed by staining with an APC-conjugated anti-mouse CD47 antibody. Similar to human αCD47-G1 (Fig. 1B), flow cytometry analysis showed a dose-dependent decrease of the APC signal when cells were preincubated with increasing concentrations of αmCD47-G2b (Fig. 5A). Murine macrophage phagocytosis and NK cell cytotoxicity against ID8 cells were measured. The results showed that supernatants from OV-αmCD47-G2b- and OV-αmCD47-G3-infected cells significantly enhanced macrophage phagocytosis against ID8 cells compared to those from OV-Q1-infected cells, yet supernatants from OV-αmCD47-G2b-infected cells were superior to those from OV-αmCD47-G3-infected cells (Fig. 5B). These results suggest that the increased phagocytotic effect of αmCD47-G2b over control groups is dependent on both blockade of “don’t eat me” signaling and ADCP, while the effect of αmCD47-G3 may be mainly from blockade of “don’t eat me” signaling. For NK cell cytotoxicity assay, only supernatants from OV-αmCD47-G2b-infected cells activated murine NK cell ADCC against ID8 cells (Fig. 5C). For evaluating the virotherapy efficacy of OV-αmCD47-G2b and OV-αmCD47-G3, an immunocompetent ovarian cancer metastasis mouse model was established. Similar to the human version of OV-αCD47-G1, administration of OV-αmCD47-G2b significantly prolonged the median survival of mice when compared to OV-αmCD47-G3 or OV-Q1 (Fig. 5D and S9). Different from the result of human versions in the ID8-hCD47 model where the murine CD47-SIRPα axis-mediated “don’t eat me signal” could not be blocked (Fig. 4B), OV-αmCD47-G3 treatment showed a significantly stronger anti-tumor effect compared to OV-Q1 treatment, exhibiting the effect of blocking the murine CD47-SIRPα axis-mediated “don’t eat me” signal (Fig. 5D and S9).

To clarify the role of NK cells and macrophages in OV-αmCD47-G2b virotherapy, we repeated the survival studies with NK cell depletion and macrophage depletion separately in the ID8 immunocompetent mouse model treated with OV-αmCD47-G2b. NK cell depletion significantly shortened the survival of OV-αmCD47-G2b-treated mice compared to OV-αmCD47-G2b-treated mice without NK cell depletion (Fig. 5E). Macrophage depletion also significantly shortened the survival of OV-αmCD47-G2b-treated mice when compared to OV-αmCD47-G2b-treated mice without macrophage depletion (Fig. 5F). These data indicate that both macrophages and NK cells mediate the effects of the OV expressing αmCD47-G2b in improving survival of mice with ovarian cancer.

The cells isolated from the tumor, liver and kidney were also analyzed. Compared to saline, OV-Q1, and OV-αmCD47-G3, OV-αmCD47-G2b significantly reduced the tumor cell numbers in the liver and kidney (Fig. 6A and B). Different from the result of human versions (Fig. 4D and S5D), OV-αmCD47-G3 treatment also decreased the tumor cell numbers in the liver and kidney compared to the OV-Q1 (Fig. 6A and B), which validated the survival data (Fig. 5D). The immune responses were also analyzed in the tumor, liver, and kidney. Similar to the human version of OV-αCD47, administration of OVs promoted the infiltration of macrophages, NK cells, and T cells into the tumor microenvironment. However, there was no difference among the three OVs in tumors in the abdomen, liver, and kidney (Fig. S10A–C). We also detected the percentages of M1 and M2 types of macrophages. In tumors from the abdomen, liver, and kidney, OV-αmCD47-G2b and OV-αmCD47-G3 treatments significantly decreased the number of M2 type macrophages and increased the number of M1 type macrophages compared to saline and OV-Q1 treatment (Fig. 6B, C and Fig. S11). Similar to the human version of OV-αCD47-G1(Fig. 4F,4H and S7E), the percentages of $CD69^+$ NK cells in tumors from the abdomen, liver and kidney were significantly increased in the OV-αmCD47-G2b group, indicating that OV-αmCD47-G2b administration activated NK cells *in vivo* (Fig. 6D–H, and Fig. S11).

We also performed a flow cytometric assessment of the amount of $CD4^+$, $CD8^+$, and Treg T cell in the spleen of mice treated with OV-Q1, OV-αmCD47-G2b, OV-αmCD47-G3, or saline control in the fully immunocompetent model. We found that after treatment with each of the three oHSVs (OV-Q1, OV-αmCD47-G2b, and OV-αmCD47-G3), there was no difference of $CD4^+$ T cells and Tregs. However, $CD8^+$ T cells were significantly increased following treatment with OV-αmCD47-G2b compared to the groups treated with OV-Q1 or OV-αmCD47-G3 (Fig. S10D). We also assessed IFNγ and granzyme B secretion of $CD8^+$ T cells in the spleen. The results showed that after treatment with each of the above three oHSVs, IFNγ and granzyme B secretion were increased without differences among those three oHSV treatments (Fig. S10E). We also analyzed anti-viral immune responses after OV-αmCD47-G2b treatment by measuring anti-HSV-1 specific $CD8^+$ T cell percentages in the spleen and anti-HSV-1 specific antibodies in the peripheral blood in this model. The anti-HSV-1 specific $CD8^+$ T cells were assessed by flow cytometry using the HSV-1 glycoprotein B tetramer. We found that after treatment with each of the above three oHSVs, anti-HSV-1 specific $CD8^+$ T cells were increased, while there was no difference among these three groups (Fig. S12A). Furthermore, the levels of anti-HSV-1 specific antibodies were similar among the three groups (Fig. S12B). Therefore, our data indicate that OV-αmCD47-G2b has no effect on enhancing anti-viral effects and clearance when compared

to OV-Q1. We measured the αmCD47-G2b antibody concentration at the tumor sites in the abdomen and the peripheral blood of the mice treated with 1×10^6 PFU OV-αmCD47-G2b by ELISA. Results showed that αmCD47-G2b antibody concentrations were significantly much higher at the tumor sites than in sera at each of the indicated time points (Fig. S13).

Collectively, OV-αmCD47-G2b showed the strongest anti-tumor effect compared to OV-αmCD47-G3 or OV-Q1 in an immunocompetent ovarian cancer metastasis mouse model, correlating to promoting macrophages polarizing towards M1 type and NK cell activation but lacking substantial adaptive immune responses.

OV expressing a CD47 antibody is superior to the antibody alone and shows a better effect when combined with a PD-L1 antibody

We compared the ability of αmCD47-G2b and OV-αmCD47-G2b on prolonging survival of mice bearing ID8 tumors. For this purpose, wild-type C57BL/6 mice were intraperitoneally injected with 2×10^6 ID8 cells. Four days later, mice were intraperitoneally injected with 1×10^6 PFU of OV-αmCD47-G2b or 150 μg of purified αmCD47-G2b. Saline was injected as control. The amount of antibody was calculated based on the data from Figure 1C in order to make certain the two groups had a similar amount of antibodies. Both αmCD47-G2b and OV-αmCD47-G2b treatments prolonged the survival of mice compared to saline treatment. However, prolongation of survival was significantly greater in tumor-bearing mice treated with OV-αmCD47-G2b when compared to tumor-bearing mice treated with αmCD47-G2b (Fig. 7A), which strengthens our hypothesis that OV-αmCD47-G2b treatment leads to: (1) direct tumor lysis by oHSVs; (2) the critical role of the innate immune cell infiltration and activation within the tumor microenvironment by oHSVs.

To enhance the adaptive immune responses in our system, we performed combination therapy with anti-PD-L1 antibody in the immunocompetent mouse model *in vivo*. For this purpose, we analyzed PD-L1 expression of ID8 ovarian tumor cells after OV-Q1 or OV-αmCD47-G2b infection *in vitro*. Our data showed that PD-L1 expression was increased after oHSV infection (Fig. 7B). Therefore, in an *in vivo* assay, anti-mPD-L1 mAb or control vehicle was injected 24 hours after OV-αmCD47-G2b treatment. Our data showed that compared to single reagent treatments, the OV-αmCD47-G2b and anti-PD-L1 mAb combination therapy significantly prolonged survival in mice bearing with ID8 ovarian tumor (Fig. 7C).

Discussion

In this study, we combined a monoclonal antibody (mAb) and oncolytic virus into a single agent to develop an innovative antibody delivery system to improve the efficacy of ovarian cancer therapy. OV-αCD47-G1 not only directly lyses tumor cells but also activates NK cell ADCC and macrophage ADCP function *in vitro*. Furthermore, OV-αCD47-G1 also blocked the “don’t eat me” signal normally mediated by the interaction between SIRPα on macrophages and CD47 on ovarian tumor cells, respectively. Therefore, OV-αCD47-G1 treatment significantly improved the virotherapy efficacy against ovarian tumors *in vivo.*

In our study, the anti-CD47 antibody and herpes simplex oncolytic virus were selected to construct the OV-αCD47-G1 and OV-αCD47-G4, which are designed to secrete αCD47-G1 and αCD47-G4, respectively, to the ovarian cancer tumor microenvironment after OVs administration. CD47 is highly expressed on surfaces of numerous types of tumor cells, including ovarian cancer, which binds to its receptor, SIRPα on the surface of macrophages. This binding results in a “don’t eat me” signal to macrophages and protects tumor cells from being killed by the former (5). Consistent with this concept, clinically used anti-CD47 antibodies have been developed to enhance the phagocytosis of cancer cells and are actively being tested in numerous clinical and preclinical studies (5,22,27,28). Furthermore, some oncolytic viruses have been engineered by fusing the SIRPα ectodomain to human IgG1 or IgG4 Fc to block the CD47- SIRPα axis (29,30).

Macrophages play key roles in tumor progression. Because of the different origins and local tumor microenvironment, tumor-associated macrophages (TAMs) act in diverse roles. Therefore, macrophages are potential therapeutic targets for anti-tumor therapy. Indeed, talimogene laherparepvec (T-VEC), the first FDA-approved oHSV for virotherapy, expresses granulocyte-macrophage colony-stimulating factor to increase tumor-antigen presentation by dendritic cells and promote macrophage accumulation (31). By secreting several cytokines or growth factors, TAMs could induce angiogenesis and promote tumor cell invasion (32). The chemokines producing by TAMs can enhance different immune cell infiltration into the TME (33). Because of the heterogeneity and plasticity, macrophages are identified into M1 and M2 types macrophages, which play extremely different roles in regulating inflammation and tumor development (34–36). M1 type macrophage could mediate resistance against tumors by secreting IL-6, iNOS, while M2 type macrophage work as a tumor promoter by secreting IL-10, Arg 1 as well as TGF-β and VEGF that induces angiogenesis (37). It has been reported that anti-CD47 treatment increases M1-polarizied macrophages in glioblastoma treatment (24). Our study showed that OV-αCD47, especially OV-αCD47-G1 and OV-αmCD47-G2b, can decrease the percentages of M2 type macrophage and increase the M1 type macrophage percentages, which restrain tumor progression.

Many studies focused on the role of T cells and NK cells on tumor clearance. However, macrophages play an important role in recognizing and depleting damaged and aged cells (38). Phagocytosis by macrophages initiates one type of innate immune responses. There are a number of phagocytic receptors, such as mannose receptors, complement receptors, recognizing the pathogens (39). Fc receptors binding with specific antibodies can also stimulate a strong phagocytosis effect (40). Furthermore, studies found that SIRPα is an important negative receptor on macrophage phagocytosis by binding to CD47 on tumor cells (5). Thus, many studies work on inhibiting the SIRPα-CD47 signal pathway to control tumor progression (5,12,41,42). In our study, we combined the SIRPα-CD47 signal pathway with Fc receptor function to activate macrophage phagocytosis. Our results demonstrated that OV-αCD47-G1 and OV-αmCD47-G2b, both of which can block the SIRPα-CD47 signaling pathway and stimulate Fc receptors, are more effective than OV-αCD47-G4 and OV-αmCD47-G3, respectively, both of which can only affect the SIRPα-CD47 signaling pathway in inhibiting tumor progression. Like PD-1 on T cells, SIRPα is a checkpoint on macrophages. Although our data show that OVs expressing a full-length CD47 antibody does not substantially modulate adaptive immune responses, combination of

the virus expressing such an antibody with an Fc function and a PD-L1 antibody to block PD-1 checkpoint on T cells shows an improved outcome compared to the corresponding monotherapy. Therefore, the oHSV expressing a full-length anti-CD47 antibody with an Fc function should likely be considered for translation into the clinic for the treatment of ovarian cancer as a single agent or combined with another effective therapy. For this purpose, we have manufactured OV-αCD47-G1 in our institutional good manufacturing practices (GMP) facility.

In the last 20 years, mAb-based drugs have been proven to be effective and widely used for treating hematologic malignancies and solid tumors. However, some limitations exist, which restrain its applications (43,44). One limitation is the poor intratumoral distribution after administration. A mAb drug administrated through a traditional mAb delivery route, such as intravenous (i.v.), subcutaneous (s.c.), or intramuscular will mainly stay in the peripheral circulatory system with low levels of accumulation in the tumor microenvironment. In addition, peripheral circulation of the antibodies results in systemic off-target side effects. If a mAb has long half-life, it would worsen toxicities. Therefore, anti-tumor mAbs were developed on an IgG4 scaffold to minimize the Fc-dependent effect to limit the potential toxicity, but this scaffold diminishes their anti-tumor effects due to limited Fc receptor-mediated anti-tumor immune responses (45,46). Similarly, several anti-CD47 antibodies are constructed on the IgG4 scaffold to minimize the Fc receptor-dependent effect and to avoid the side effect from off-targeting (5). Using our oncolytic virus-based antibody delivery system, the anti-CD47 antibody can be directly and accurately delivered to the tumor microenvironment. This should enhance the availability of mAbs and limit the potential toxicity, thus providing an opportunity to use a stronger scaffold such as IgG1 to harness and maximize Fc receptor-mediated anti-tumor effects.

In summary, we have developed an effective oHSV-based approach via engineering a transgene expressing a full-length anti-CD47 Ab on an IgG1 scaffold to treat ovarian cancer. The approach has multifaceted functions, combining direct tumor lysis, innate immune infiltration and activation, immune checkpoint inhibition of macrophages, and Fc-dependent innate immune cell cytotoxic functions. Our approach significantly enhances the overall efficacy of both oncolytic virotherapy and mAb therapy for the treatment of ovarian cancer in preclinical mouse models.

Supplementary Material

Refer to Web version on PubMed Central for supplementary material.

Acknowledgments

This work was supported by grants from the NIH (NS106170, AI129582, CA247550, CA163205, CA223400, CA265095, CA210087, CA20175, and CA255250), the Leukemia & Lymphoma Society (1364-19), California Institute for Regenerative Medicine (DISC2COVID19-11947), the Breast Cancer Alliance, Markel Friedman Accelerator Fund, and the V Foundation for Cancer Research V Scholar Award. The authors thank the NIH Tetramer Core Facility for providing the herpes simplex virus type 1 glycoprotein B tetramer.

References

1. Stewart C, Ralyea C, Lockwood S. Ovarian Cancer: An Integrated Review. Semin Oncol Nurs 2019;35(2):151–6 doi 10.1016/j.soncn.2019.02.001. [PubMed: 30867104]
2. Roett MA, Evans P. Ovarian cancer: an overview. Am Fam Physician 2009;80(6):609–16.
3. Kossai M, Leary A, Scoazec JY, Genestie C. Ovarian Cancer: A Heterogeneous Disease. Pathobiology 2018;85(1–2):41–9 doi 10.1159/000479006. [PubMed: 29020678]
4. Grunewald T, Ledermann JA. Targeted Therapies for Ovarian Cancer. Best Pract Res Clin Obstet Gynaecol 2017;41:139–52 doi 10.1016/j.bpobgyn.2016.12.001. [PubMed: 28111228]
5. Willingham SB, Volkmer JP, Gentles AJ, Sahoo D, Dalerba P, Mitra SS, et al. The CD47-signal regulatory protein alpha (SIRPa) interaction is a therapeutic target for human solid tumors. Proc Natl Acad Sci U S A 2012;109(17):6662–7 doi 10.1073/pnas.1121623109. [PubMed: 22451913]
6. Brightwell RM, Grzankowski KS, Lele S, Eng K, Arshad M, Chen H, et al. The CD47 “don’t eat me signal” is highly expressed in human ovarian cancer. Gynecol Oncol 2016;143(2):393–7 doi 10.1016/j.ygyno.2016.08.325. [PubMed: 27569584]
7. Logtenberg MEW, Scheeren FA, Schumacher TN. The CD47-SIRPalpha Immune Checkpoint. Immunity 2020;52(5):742–52 doi 10.1016/j.immuni.2020.04.011. [PubMed: 32433947]
8. Kojima Y, Volkmer JP, McKenna K, Civelek M, Lusis AJ, Miller CL, et al. CD47-blocking antibodies restore phagocytosis and prevent atherosclerosis. Nature 2016;536(7614):86–90 doi 10.1038/nature18935. [PubMed: 27437576]
9. Feng M, Jiang W, Kim BYS, Zhang CC, Fu YX, Weissman IL. Phagocytosis checkpoints as new targets for cancer immunotherapy. Nat Rev Cancer 2019;19(10):568–86 doi 10.1038/s41568-019-0183-z. [PubMed: 31462760]
10. Cao X, Li B, Chen J, Dang J, Chen S, Gunes EG, et al. Effect of cabazitaxel on macrophages improves CD47-targeted immunotherapy for triple-negative breast cancer. J Immunother Cancer 2021;9(3) doi 10.1136/jitc-2020-002022.
11. Kaur S, Cicalese KV, Bannerjee R, Roberts DD. Preclinical and Clinical Development of Therapeutic Antibodies Targeting Functions of CD47 in the Tumor Microenvironment. Antib Ther 2020;3(3):179–92 doi 10.1093/abt/tbaa017. [PubMed: 33244513]
12. Zhang W, Huang Q, Xiao W, Zhao Y, Pi J, Xu H, et al. Advances in Anti-Tumor Treatments Targeting the CD47/SIRPalpha Axis. Front Immunol 2020;11:18 doi 10.3389/fimmu.2020.00018. [PubMed: 32082311]
13. Adams GP, Weiner LM. Monoclonal antibody therapy of cancer. Nat Biotechnol 2005;23(9):1147–57 doi 10.1038/nbt1137. [PubMed: 16151408]
14. Touzeau C, Moreau P, Dumontet C. Monoclonal antibody therapy in multiple myeloma. Leukemia 2017;31(5):1039–47 doi 10.1038/leu.2017.60. [PubMed: 28210004]
15. Xu B, Ma R, Russell L, Yoo JY, Han J, Cui H, et al. An oncolytic herpesvirus expressing E-cadherin improves survival in mouse models of glioblastoma. Nat Biotechnol 2018 doi 10.1038/nbt.4302.
16. Han J, Chen X, Chu J, Xu B, Meisen WH, Chen L, et al. TGFbeta Treatment Enhances Glioblastoma Virotherapy by Inhibiting the Innate Immune Response. Cancer Res 2015;75(24):5273–82 doi 10.1158/0008-5472.CAN-15-0894. [PubMed: 26631269]
17. Chen X, Han J, Chu J, Zhang L, Zhang J, Chen C, et al. A combinational therapy of EGFR-CAR NK cells and oncolytic herpes simplex virus 1 for breast cancer brain metastases. Oncotarget 2016;7(19):27764–77 doi 10.18632/oncotarget.8526. [PubMed: 27050072]
18. Ma R, Lu T, Li Z, Teng KY, Mansour AG, Yu M, et al. An oncolytic virus expressing IL-15/IL-15Ralpha combined with off-the-shelf EGFR-CAR NK cells targets glioblastoma. Cancer Res 2021 doi 10.1158/0008-5472.CAN-21-0035.
19. Terada K, Wakimoto H, Tyminski E, Chiocca EA, Saeki Y. Development of a rapid method to generate multiple oncolytic HSV vectors and their in vivo evaluation using syngeneic mouse tumor models. Gene Ther 2006;13(8):705–14 doi 10.1038/sj.gt.3302717. [PubMed: 16421599]
20. Chen L, Mao H, Zhang J, Chu J, Devine S, Caligiuri MA, et al. Targeting FLT3 by chimeric antigen receptor T cells for the treatment of acute myeloid leukemia. Leukemia 2017;31(8):1830–4 doi 10.1038/leu.2017.147. [PubMed: 28496177]

21. Wang Y, Chu J, Yi P, Dong W, Saultz J, Wang Y, et al. SMAD4 promotes TGF-beta-independent NK cell homeostasis and maturation and antitumor immunity. J Clin Invest 2018;128(11):5123–36 doi 10.1172/JCI121227. [PubMed: 30183689]
22. Liu J, Wang L, Zhao F, Tseng S, Narayanan C, Shura L, et al. Pre-Clinical Development of a Humanized Anti-CD47 Antibody with Anti-Cancer Therapeutic Potential. PLoS One 2015;10(9):e0137345 doi 10.1371/journal.pone.0137345.
23. Kitange GJ, Carlson BL, Schroeder MA, Grogan PT, Lamont JD, Decker PA, et al. Induction of MGMT expression is associated with temozolomide resistance in glioblastoma xenografts. Neuro Oncol 2009;11(3):281–91 doi 10.1215/15228517-2008-090. [PubMed: 18952979]
24. Zhang M, Hutter G, Kahn SA, Azad TD, Gholamin S, Xu CY, et al. Anti-CD47 Treatment Stimulates Phagocytosis of Glioblastoma by M1 and M2 Polarized Macrophages and Promotes M1 Polarized Macrophages In Vivo. PLoS One 2016;11(4):e0153550 doi 10.1371/journal.pone.0153550.
25. Sockolosky JT, Dougan M, Ingram JR, Ho CC, Kauke MJ, Almo SC, et al. Durable antitumor responses to CD47 blockade require adaptive immune stimulation. Proc Natl Acad Sci U S A 2016;113(19):E2646–54 doi 10.1073/pnas.1604268113. [PubMed: 27091975]
26. Bruhns P. Properties of mouse and human IgG receptors and their contribution to disease models. Blood 2012;119(24):5640–9 doi 10.1182/blood-2012-01-380121. [PubMed: 22535666]
27. Veillette A, Chen J. SIRPalpha-CD47 Immune Checkpoint Blockade in Anticancer Therapy. Trends Immunol 2018;39(3):173–84 doi 10.1016/j.it.2017.12.005. [PubMed: 29336991]
28. Sikic BI, Lakhani N, Patnaik A, Shah SA, Chandana SR, Rasco D, et al. First-in-Human, First-in-Class Phase I Trial of the Anti-CD47 Antibody Hu5F9-G4 in Patients With Advanced Cancers. J Clin Oncol 2019;37(12):946–53 doi 10.1200/JCO.18.02018. [PubMed: 30811285]
29. Huang Y, Lv SQ, Liu PY, Ye ZL, Yang H, Li LF, et al. A SIRPalpha-Fc fusion protein enhances the antitumor effect of oncolytic adenovirus against ovarian cancer. Mol Oncol 2020;14(3):657–68 doi 10.1002/1878-0261.12628. [PubMed: 31899582]
30. Cao F, Nguyen P, Hong B, DeRenzo C, Rainusso NC, Rodriguez Cruz T, et al. Engineering Oncolytic Vaccinia Virus to redirect Macrophages to Tumor Cells. Adv Cell Gene Ther 2021;4(2) doi 10.1002/acg2.99.
31. Conry RM, Westbrook B, McKee S, Norwood TG. Talimogene laherparepvec: First in class oncolytic virotherapy. Hum Vaccin Immunother 2018;14(4):839–46 doi 10.1080/21645515.2017.1412896. [PubMed: 29420123]
32. Qian BZ, Pollard JW. Macrophage diversity enhances tumor progression and metastasis. Cell 2010;141(1):39–51 doi 10.1016/j.cell.2010.03.014. [PubMed: 20371344]
33. Balkwill FR, Mantovani A. Cancer-related inflammation: common themes and therapeutic opportunities. Semin Cancer Biol 2012;22(1):33–40 doi 10.1016/j.semcancer.2011.12.005. [PubMed: 22210179]
34. Gordon S. Alternative activation of macrophages. Nature Reviews Immunology 2003;3(1):23–35 doi 10.1038/nri978.
35. Mantovani A, Sozzani S, Locati M, Allavena P, Sica A. Macrophage polarization: tumor-associated macrophages as a paradigm for polarized M2 mononuclear phagocytes. Trends Immunol 2002;23(11):549–55 doi 10.1016/s1471-4906(02)02302-5. [PubMed: 12401408]
36. Mantovani A, Sica A, Sozzani S, Allavena P, Vecchi A, Locati M. The chemokine system in diverse forms of macrophage activation and polarization. Trends Immunol 2004;25(12):677–86 doi 10.1016/j.it.2004.09.015. [PubMed: 15530839]
37. Noy R, Pollard JW. Tumor-associated macrophages: from mechanisms to therapy. Immunity 2014;41(1):49–61 doi 10.1016/j.immuni.2014.06.010. [PubMed: 25035953]
38. Jaiswal S, Chao MP, Majeti R, Weissman IL. Macrophages as mediators of tumor immunosurveillance. Trends Immunol 2010;31(6):212–9 doi 10.1016/j.it.2010.04.001. [PubMed: 20452821]
39. Aderem A, Underhill DM. Mechanisms of phagocytosis in macrophages. Annu Rev Immunol 1999;17:593–623 doi 10.1146/annurev.immunol.17.1.593. [PubMed: 10358769]

40. Mellman IS, Plutner H, Steinman RM, Unkeless JC, Cohn ZA. Internalization and degradation of macrophage Fc receptors during receptor-mediated phagocytosis. J Cell Biol 1983;96(3):887–95 doi 10.1083/jcb.96.3.887. [PubMed: 6833386]

41. Fu X, Tao L, Zhang X. Genetically coating oncolytic herpes simplex virus with CD47 allows efficient systemic delivery and prolongs virus persistence at tumor site. Oncotarget 2018;9(77):34543–53 doi 10.18632/oncotarget.26167. [PubMed: 30349648]

42. von Roemeling CA, Wang Y, Qie Y, Yuan H, Zhao H, Liu X, et al. Therapeutic modulation of phagocytosis in glioblastoma can activate both innate and adaptive antitumour immunity. Nat Commun 2020;11(1):1508 doi 10.1038/s41467-020-15129-8. [PubMed: 32198351]

43. Cruz E, Kayser V. Monoclonal antibody therapy of solid tumors: clinical limitations and novel strategies to enhance treatment efficacy. Biologics 2019;13:33–51 doi 10.2147/BTT.S166310. [PubMed: 31118560]

44. Melero I, Hervas-Stubbs S, Glennie M, Pardoll DM, Chen L. Immunostimulatory monoclonal antibodies for cancer therapy. Nat Rev Cancer 2007;7(2):95–106 doi 10.1038/nrc2051. [PubMed: 17251916]

45. Crescioli S, Correa I, Karagiannis P, Davies AM, Sutton BJ, Nestle FO, et al. IgG4 Characteristics and Functions in Cancer Immunity. Curr Allergy Asthma Rep 2016;16(1):7 doi 10.1007/s11882-015-0580-7. [PubMed: 26742760]

46. Isaacs JD, Wing MG, Greenwood JD, Hazleman BL, Hale G, Waldmann H. A therapeutic human IgG4 monoclonal antibody that depletes target cells in humans. Clin Exp Immunol 1996;106(3):427–33 doi 10.1046/j.1365-2249.1996.d01-876.x. [PubMed: 8973608]

Statement of translational relevance

Oncolytic virus (OV) therapies and monoclonal antibody (mAb) therapies are becoming attractive therapeutic agents for treating cancer. Many types of cancer cells overexpress an important immune checkpoint, CD47, which binds to its receptor, SIRPα, on macrophages to promote immune suppression. Anti-CD47 monoclonal antibodies are being actively evaluated in clinical trials. In this study, we combined oncolytic virotherapy with antibody therapy into a single therapeutic agent to preclinically treat ovarian cancer by generating an OV expressing a full-length anti-CD47 mAb (OV-αCD47). We showed that OV-αCD47, especially with an IgG1 scaffold (OV-αCD47-G1), improved survival in xenograft and immunocompetent mouse models of ovarian cancer by activating NK cell cytotoxicity and enhancing macrophage phagocytosis. Therefore, using an oncolytic virus to encode and deliver a full-length mAb in cancer patients may improve oncolytic virotherapy by enhancing anti-tumor immunity.

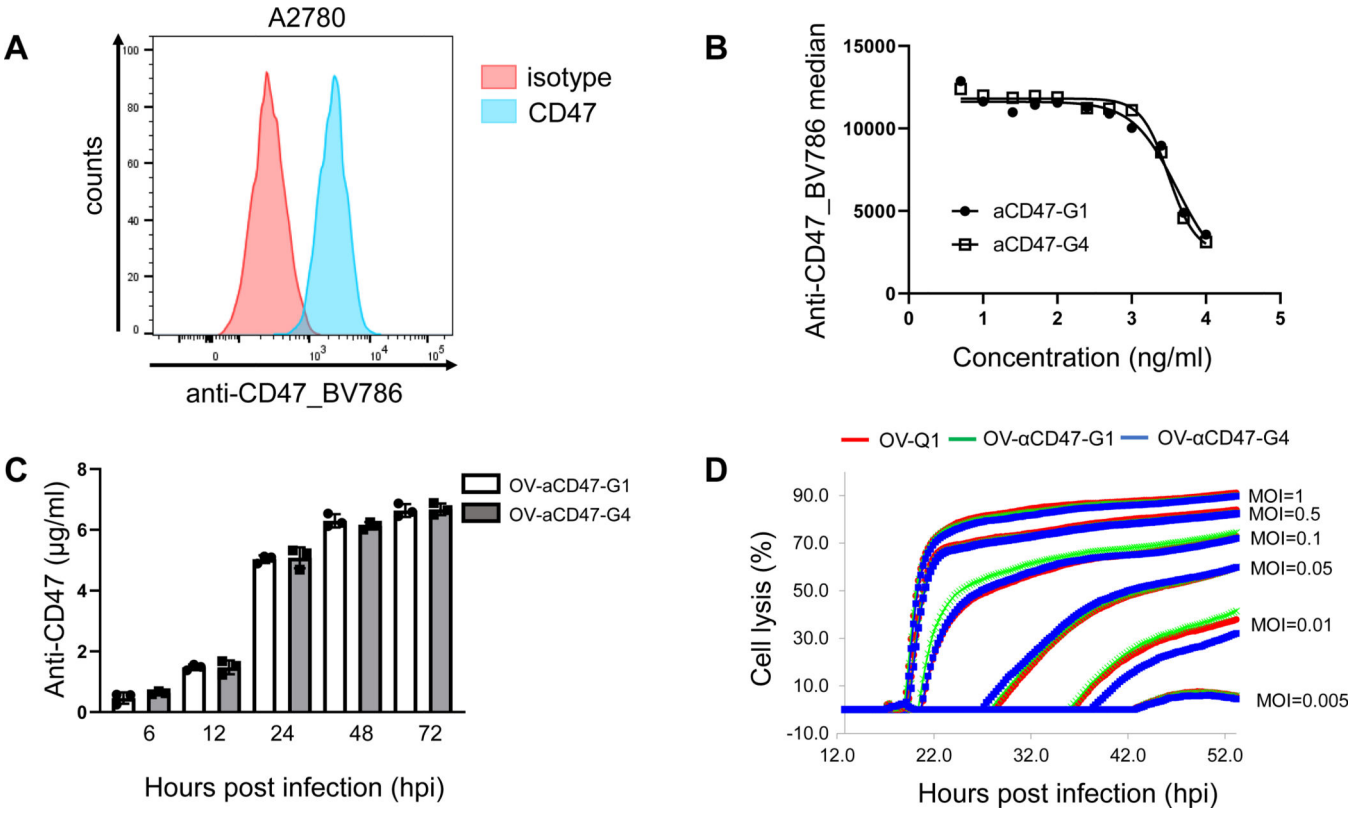

Figure 1. Characterization of OV-αCD47-G1 and OV-αCD47-G4.

(**A**) Flow cytometric assay of CD47 expression on A2780 cells. (**B**) Inhibition of anti-CD47 mAb binding by αCD47-G1 and αCD47-G4 mAbs purified from lentiviral infected CHO cells. A2780 cells were incubated with different concentrations of unlabeled αCD47-G1 or αCD47-G4 mAb followed by incubation with a conjugated anti-human CD47 and assessed by flow cytometry. **(C)** αCD47-G1 and αCD47-G4 yields from supernatants of OV-αCD47-G1- and OV-αCD47-G4-infected A2780 cells as determined by ELISA assay using standards of serial dilutions of the corresponding antibody purified from lentiviral infected CHO cells. (**D**) A2780 cells were infected with OV-Q1, OV-αCD47-G1 or OV-αCD47-G4 at the indicated MOIs. Cell lysis was analyzed by real-time cell analysis (RTCA). Experiments in A are representative of three independent experiments with similar data. Error bars represent standard deviations (SD). Data were presented as mean values +/− SD.

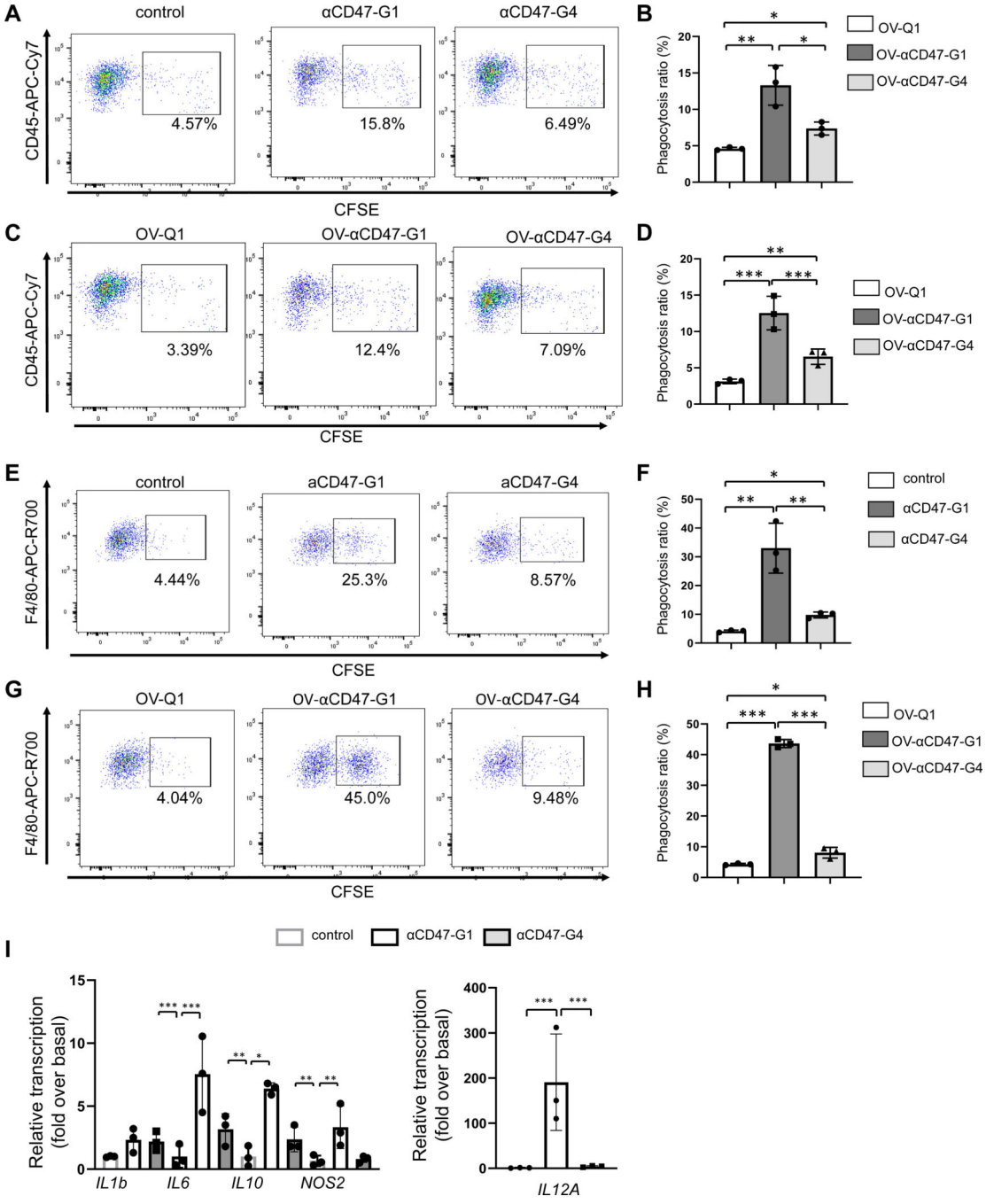

Figure 2. αCD47-G1 and αCD47-G4 induce phagocytosis of A2780 ovarian cells by macrophages.

(A-B) Examination of the effect of 5 μg/ml of αCD47-G1 and αCD47-G4 purified from lentiviral- infected CHO cells on phagocytosis of A2780 cells by primary human macrophages. **(C-D)** The supernatants from OV-αCD47-G1- and OV-αCD47-G4-infected A2780 cells induce phagocytosis against A2780 cells by primary human macrophages. Phagocytosis was assessed by flow cytometry. **(E-F)** Examination of the effect of 5 μg/ml of αCD47-G1 and αCD47-G4 purified from lentiviral-infected CHO cells on phagocytosis

of A2780 cells by bone marrow-derived macrophages (BMDMs). Percentages of BMDM phagocytosis of A2780 cells ($CD11b^+CFSE^+$) were determined by flow cytometry. **(G-H)** The supernatant from OV-αCD47-G1- and OV-αCD47-G4-infected A2780 cells induce phagocytosis against A2780 cells by BMDMs. Phagocytosis was assessed by flow cytometry. (**I**) Primary human macrophages were cocultured with A2780 cells at a ratio of 1:1 with or without αCD47-G1 or αCD47-G4 for 6 hours after which gene transcripts were quantified. All experiments were repeated using 3 human donors or mice with similar results. Statistical analyses were performed by one-way ANOVA with P values corrected for multiple comparisons by Bonferroni method. *$P \leq 0.05$; **$P \leq 0.01$; ***$P \leq 0.001$. Data were presented as mean values +/− SD.

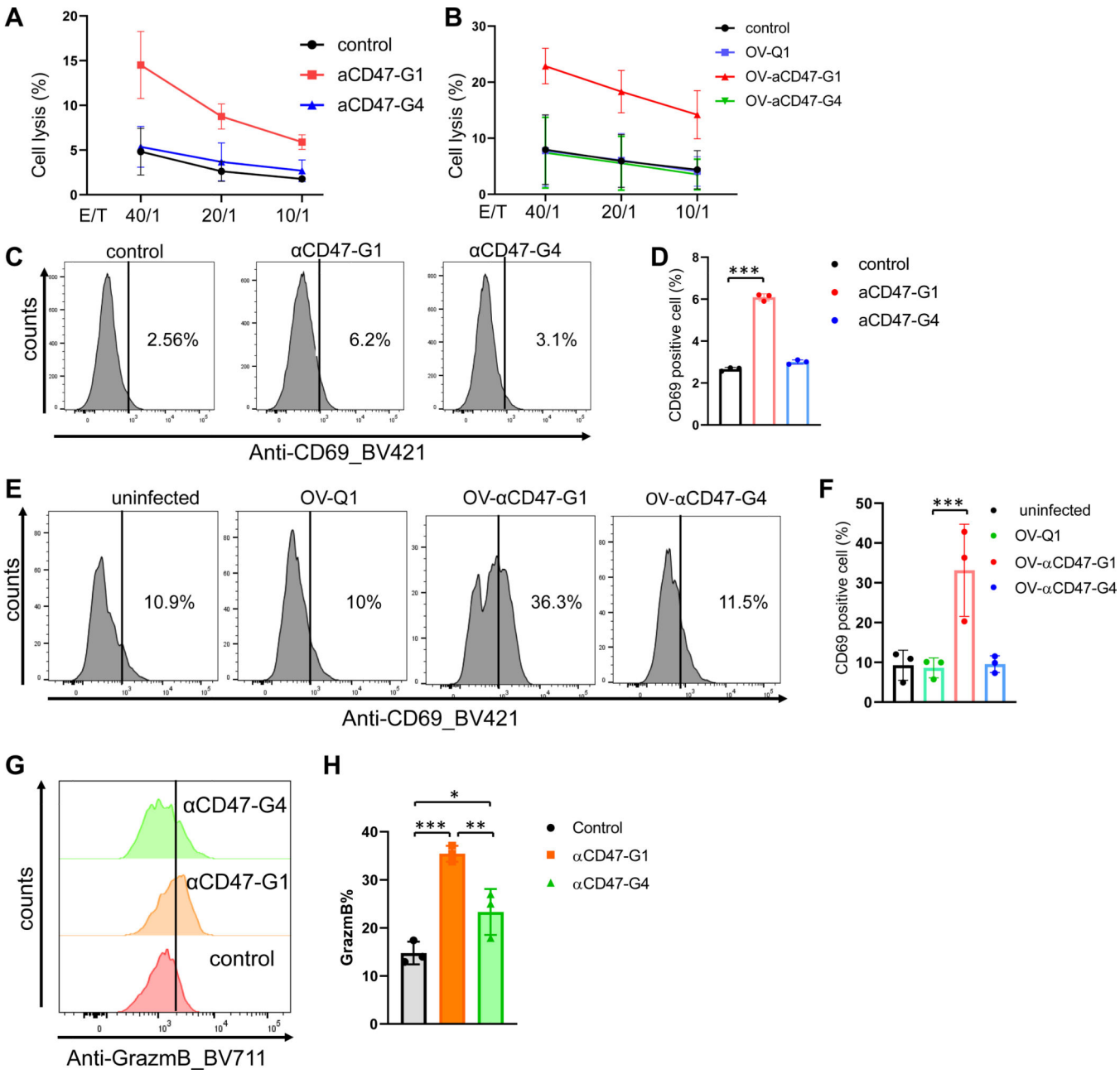

Figure 3. αCD47-G1 but not αCD47-G4 induces cytotoxicity of human NK cells against ovarian cancer cells.

(A) Cytotoxicity of human primary NK cells against αCD47-G1- and αCD47-G4-treated A2780 human ovarian cancer cells. PBS was the control. Control vs. αCD47-G1 ***P ≤ 0.001; αCD47-G1 vs. αCD47-G4 *P ≤ 0.05. **(B)** Cytotoxicity of human primary NK cells against A2780 cells that were treated with supernatants from OV-Q1-, OV-αCD47-G1- or OV-αCD47-G4-infected A2780 cells. OV-Q1 vs. OV-αCD47-G1, ***P ≤ 0.001; OV-αCD47-G1 vs. OV-αCD47-G4, ***P ≤ 0.001. **(C)** CD69 expression of NK cells cocultured with A2780 cells that were pretreated with αCD47-G1 or αCD47-G4 was detected by flow cytometry. **(D)** Summary data of (C). **(E)** CD69 expression of NK cells

when cocultured with A2780 cells with supernatants from OV-Q1-, OV-αCD47-G1- or OV-αCD47-G4-infected A2780 cells was detected by flow cytometry. **(F)** Summary data of (E). **(G)** Granzyme B expression by NK cells cocultured with A2780 cells that were pretreated with αCD47-G1 or αCD47-G4 was detected by flow cytometry. **(H)** Summary data of (G). All experiments were performed with three donors. Error bars represent standard deviations of the means of three donors. For C to H, statistical analyses were performed by one-way ANOVA with P values corrected for multiple comparisons by Bonferroni method. *$P \leq 0.05$; **$P \leq 0.01$; ***$P \leq 0.001$. Data were presented as mean values +/− SD.

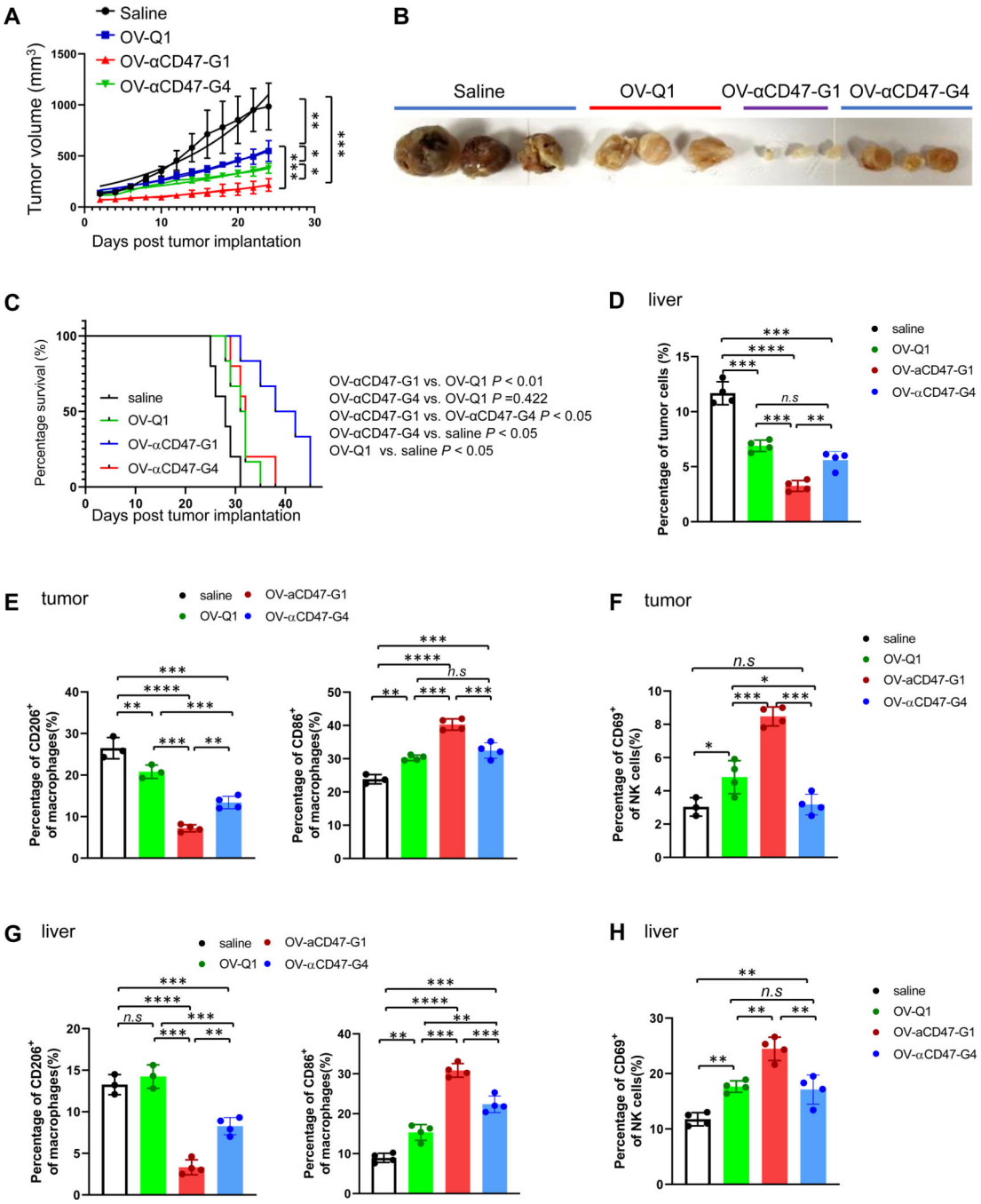

Figure 4. OV-αCD47-G1 improves the therapeutic efficacy against ovarian tumor.

An orthotopic model of human ovarian tumor was established by s.c. injection of 5×10^6 A2780 cells. Two days later, mice were intratumorally injected with a vehicle control or 1×10^5 PFU of OV-Q1, OV-αCD47-G1, or OV-αCD47-G4. **(A)** Tumor volume of ovarian tumor growth in mice with indicated treatments. **(B)** The representative tumor images from the four treatment groups. An immunocompetent ovarian cancer metastasis mouse model was established by i.p. injection of 2×10^6 ID8-hCD47 cells expressing a firefly luciferase gene and a GFP gene, following by injected with a vehicle control or 1×10^6 PFU of OV-Q1,

OV-αCD47-G1, or OV-αCD47-G4. **(C)** Survival curve of immunocompetent ovarian cancer mice with indicated treatments (n = 6 each group). Survival was estimated by the Kaplan–Meier method and compared by log-rank test (n=6 mice each group). **(D)** Percentages of tumor cells among total live cells in the liver. **(E)** M1 and M2 types of macrophages in tumors from the abdomen were measured by flow cytometry. **(F)** Percentages of $CD69^+$ NK cells in tumors in the abdomen were measured by flow cytometry. **(G-H)** Percentages of M1 and M2 types of macrophages (G) and $CD69^+$ NK cells among lymphocyte cells (H) in the liver were measured by flow cytometry. For D to H, Statistical analyses were performed by one-way ANOVA with P values corrected for multiple comparisons by Bonferroni method (n = 3 or 4 mice per group). *P ≤ 0.05; **P ≤ 0.01; ***P ≤0.001; ****P ≤ 0.0001; *n.s.* non-significant. Data were presented as mean values +/− SD.

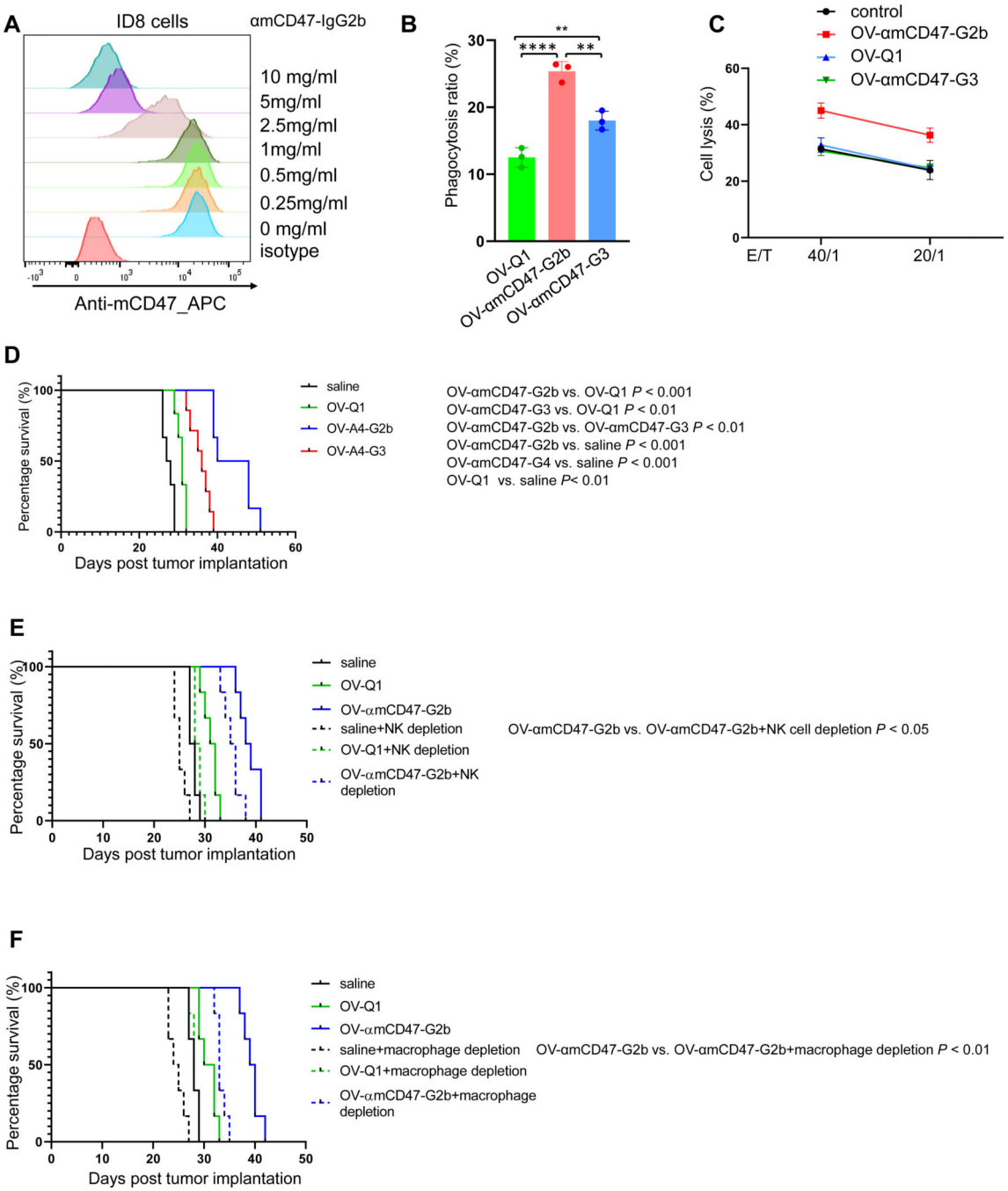

Figure 5. OV-αmCD47-G2b is efficacious to treat ovarian cancer in an immunocompetent metastasis mouse model.

(**A**) Inhibition of anti-mouse CD47 mAb binding by αmCD47-G2b mAb. ID8 cells were incubated with different concentrations of unlabeled αmCD47-G2b, followed by flow cytometry post incubation with a conjugated anti-mouse CD47. (**B**) Mouse macrophage phagocytosis induced by conditioned media from OV-αmCD47-G2b-, OV-αmCD47-G3- or OV-Q1-infected cells targeting ID8 cells, as measured by flow cytometry. (**C**) Cytotoxicity of mouse primary NK cells against ID8 cells that were treated with conditioned media

from OV-αmCD47-G2b-, OV-αmCD47-G3- or OV-Q1-infected cells, as measured by ^{51}Cr release. OV-Q1 vs. OV-αmCD47-G2b, ***P ≤ 0.001; OV-αmCD47-G2b vs. OV-αmCD47-G3, ***P ≤ 0.001. (**D**) Survival of ID8 tumor-bearing mice treated with OV-Q1, OV-αmCD47-G2b, OV-αmCD47-G3, or vehicle control (n=6 mice each group). **(E)** ID8 ovarian tumor mice were treated with OV-Q1 or OV-αmCD47-G2b with or without NK cell depletion. P < 0.05 for OV- αmCD47-G2b without NK cell depletion vs. OV-αmCD47-G2b with NK cell depletion. **(F)** ID8 ovarian tumor mice were treated with OV-Q1 or OV-αmCD47-G2b with or without macrophage depletion. P ≤ 0.01 for αmCD47-G2b without macrophage depletion vs. αmCD47-G2b with macrophage depletion. Survival was estimated by the Kaplan–Meier method and compared by log-rank test (n=6 mice each group). For B, statistical analyses were performed by one-way ANOVA with P values corrected for multiple comparisons by Bonferroni method (n = 3 mice). *P ≤ 0.05; **P ≤ 0.01; ***P ≤0.001; ****P ≤ 0.0001. Data were presented as mean values +/− SD.

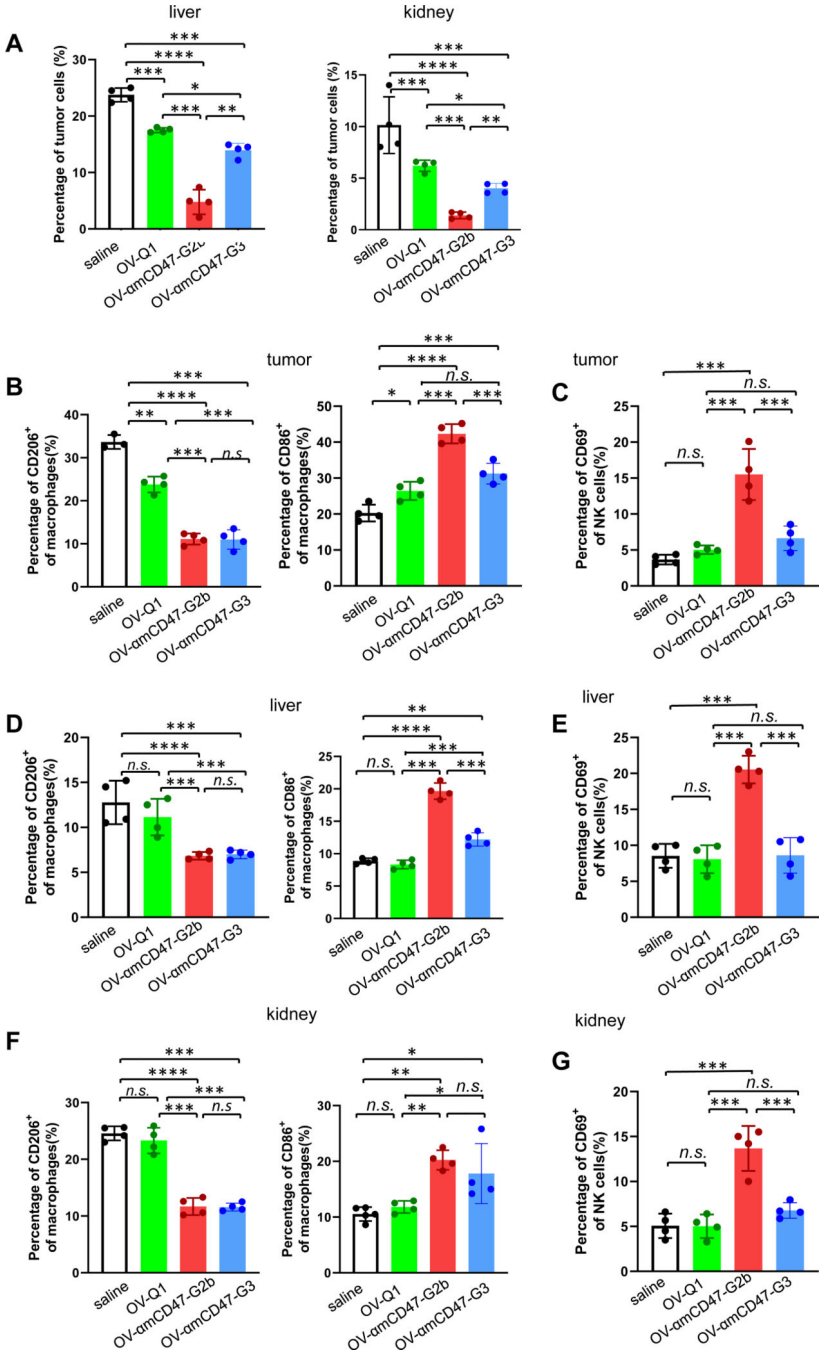

Figure 6. OV-αmCD47-G2b promotes macrophage polarization towards M1 type and NK cell activation in an immunocompetent metastasis mouse model.

(A) Percentages of tumor cells among live cells in the liver and kidney were measured by flow cytometry. **(B)** Percentages of M1 and M2 types of macrophages among lymphocyte cells in tumors from the abdomen were measured by flow cytometry. **(C)** Percentages of $CD69^+$ NK cells in tumors in the abdomen were measured by flow cytometry. **(D-E)** Percentages of M1 and M2 types macrophages (D), and percentages of $CD69^+$ NK cells among lymphocyte cells (E) in the liver were measured by flow cytometry. **(F-G)**

Percentages of M1 and M2 types macrophages (F), and percentages of $CD69^{+}$ NK cells among lymphocyte cells (G) in the kidney were measured by flow cytometry. Statistical analyses were performed by one-way ANOVA with P values corrected for multiple comparisons by Bonferroni method (n = 3 or 4 mice per group). *P ≤ 0.05; **P ≤ 0.01; ***P ≤ 0.001; ****P ≤ 0.0001; *n.s.* non-significant. Data were presented as mean values +/− SD.

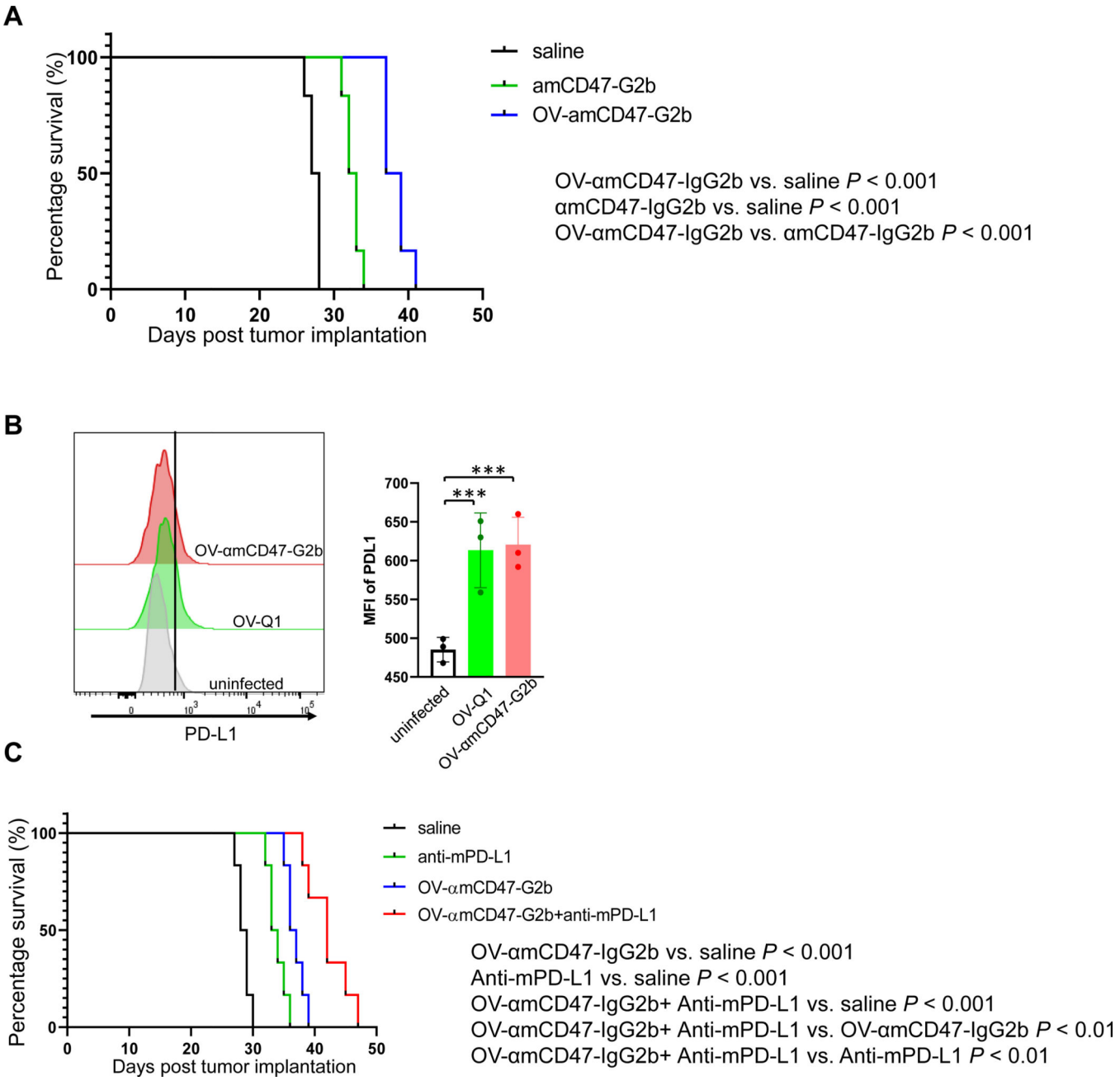

Figure 7. OV expressing a CD47 antibody is superior to the antibody alone and shows a better effect when combined with a PD-L1 antibody.

(A) Survival of ID8 tumor-bearing mice treated with OV-αmCD47-G2b, αmCD47-G2b, or vehicle control. **(B)** PD-L1 expression of ID8 ovarian tumor cells was measured by flow cytometry. Statistical analyses were performed by one-way ANOVA with P values corrected for multiple comparisons by Bonferroni method. ***P ≤ 0.001. Data were presented as mean values +/− SD. **(C)** Survival of ID8 tumor-bearing mice treated with OV-αmCD47-G2b, anti-mPD-L1 mAbs, OV-αmCD47-G2b plus anti-mPD-L1 mAbs, or vehicle control.

Survival was estimated by the Kaplan–Meier method and compared by two-side log-rank test (n = 6 animals per group).